01 Jan 2014

Nonlinear Development and Secondary Instability of Traveling Crossflow Vortices

Fei Li

Meelan M. Choudhari

Lian Duan
Missouri University of Science and Technology, duanl@mst.edu

Chau-Lyan Chang

Recommended Citation

Nonlinear development and secondary instability of traveling crossflow vortices

Fei Li,[1,a)] Meelan M. Choudhari,[1,b)] Lian Duan,[2,c)] and Chau-Lyan Chang[1,d)]
[1]*NASA Langley Research Center, Hampton, Virginia 23681, USA*
[2]*Department of Mechanical and Aerospace Engineering, Missouri University of Science and Technology, Rolla, Missouri 65409, USA*

Building upon the prior research targeting the laminar breakdown mechanisms associated with stationary crossflow instability over a swept-wing configuration, this paper investigates the secondary instability of traveling crossflow modes as an alternate scenario for transition. For the parameter range investigated herein, this alternate scenario is shown to be viable unless the initial amplitudes of the traveling crossflow instability are lower than those of the stationary modes by considerably more than one order of magnitude. The linear growth predictions based on the secondary instability theory are found to agree well with both parabolized stability equations and direct numerical simulation, and the most significant discrepancies among the various predictions are limited to spatial regions of relatively weak secondary growth, i.e., regions where the primary disturbance amplitudes are smaller in comparison to their peak values. Nonlinear effects on secondary instability evolution are also investigated and found to be initially stabilizing when they first come into play. [http://dx.doi.org/10.1063/1.4883256]

I. INTRODUCTION

The economic and environmental benefits of laminar flow technology via reduced fuel burn of transport aircraft cannot be realized without minimizing the uncertainty in drag prediction in general and transition prediction for boundary layer flows in particular. Thus, it becomes essential to develop a validated set of variable fidelity prediction tools to enable sufficiently accurate transition prediction and practical transition control for the future vehicle concepts. In particular, transition due to crossflow instability has been difficult to predict in the context of both subsonic and supersonic transports. The purpose of the present research is to investigate the transition mechanisms involving the breakdown of traveling crossflow vortices, which have received less attention than their stationary counterpart.

In general, a swept wing boundary layer can be susceptible to various types of primary instabilities such as attachment line instability,[1] stationary and traveling crossflow modes, and Tollmien-Schlichting (TS) waves. Malik *et al.*[2] studied the nonlinear development of stationary and traveling crossflow vortices and their interactions in an incompressible swept Hiemenz flow, as well as the associated temporal secondary instabilities of stationary crossflow vortices. A follow on study by Malik *et al.*[3] studied the secondary instability of stationary crossflow vortices over an essentially incompressible swept wing configuration that was the focus of a wind tunnel experiment at Arizona State University (ASU) by Reibert *et al.*[4] Gaster's relation[5] was used to convert temporal growth rates of secondary instability into spatial growth rates so as to enable predictions of associated amplification ratios (i.e., N-factors) of secondary instability waves. The predicted N-factor values were correlated with transition locations measured in the ASU experiment. The two major types of

---

a)fei.li@nasa.gov.
b)meelan.m.choudhari@nasa.gov.
c)duanl@mst.edu.
d)chau-lyan.chang@nasa.gov.

    26, 064104-1

secondary instability modes found in this case were classified as Y- and Z-modes, respectively, based on the dominant direction of mean flow shear that contributes to the energy production mechanisms associated with this instability mode. Often, the Y-direction is associated with the wall-normal direction and, therefore, the Y-modes of secondary instability correspond to modes that primarily derive their energy production mechanism from the wall-normal velocity gradient associated with a nonlinearly developed primary crossflow vortex. Similarly, the Z-mode is associated with disturbance energy production via the spanwise velocity gradient. The same classification was subsequently used in a number of follow-on papers. Koch *et al.*[6] examined the nonlinear equilibrium solutions in three-dimensional boundary layer and their secondary instability.

Direct numerical simulations involving secondary instability of stationary crossflow modes were described by Hogberg and Henningson[7] and Bonfigli and Kloker.[8] A majority of the previous studies from the literature were directed at understanding and prediction of the secondary instability modes. However, Friedrich and Kloker[9] recently described an interesting investigation that demonstrated the successful control of secondary instability via localized suction at the surface.

Regardless of which mode dominates the primary amplification stage, the other modes could play a role during the nonlinear stage and hence, influence the onset of transition. Although, in cases of practical interest, the breakdown of stationary crossflow vortices appears to be the more likely route to transition,[2,4,6–13] other scenarios involving a more significant role for the traveling crossflow instability[14–17] may become relevant under less common circumstances. These may happen either when the initial amplitudes of traveling modes become sufficiently large as a result of higher amplitude freestream disturbances or when the surface has been carefully polished to minimize the initial amplitudes of stationary crossflow modes. Wassermann and Klocker[15] studied the nonlinear saturation of traveling crossflow vortices and the associated developments of secondary instability for a flat plate configuration subject to a favorable pressure gradient. Among their findings are that the finite amplitude traveling crossflow vortices form stronger internal shear layers which are much closer to the wall than their stationary counterpart and that the secondary instability is dominated by the so called Z-modes[3] that are dominated by energy production mechanisms associated with spanwise variations (i.e., in Z-coordinate) of the underlying basic state. In a recent paper, Choudhari *et al.*[16] used nonlinear parabolized stability equations (NPSE) and linear secondary instability theory (LSIT) to analyze the traveling crossflow vortices and their secondary instability and found that, even though the traveling crossflow vortices saturate at much lower amplitudes than their stationary counterparts, the growth of secondary instabilities of the traveling crossflow vortices is at least as strong as the secondary modes of the stationary crossflow vortices when the amplitudes of the two types of primary disturbances at the respective lower branch neutral locations are comparable to each other. They also observed the Y-mode[3] secondary instability (associated with wall-normal variations of the basic state), which becomes dominant when the amplitude of the primary crossflow vortex is large. Down and White[17] studied the effect of freestream turbulence on the development of crossflow disturbances in a recent experiment and showed that increasing freestream turbulent levels promote the traveling crossflow vortices. Their paper also included a thorough review of the previous work on this topic.

The present paper stands apart from the abovementioned studies in a number of different ways. To our knowledge, it represents the first application of linear secondary instability theory to traveling crossflow vortices. Furthermore, the setting used is more general in that it is applicable to a compressible swept wing boundary layer. Finally, a formally consistent model of spatial secondary instability is presented by extending the previous work by Li and Choudhari[18,19] for the secondary instabilities of stationary crossflow vortices.

In a practical setting, the investigation of nonlinear breakdown scenarios associated with a mixed evolution of stationary and traveling crossflow modes is perhaps more important. However, as a prelude to the more complex scenario, the secondary instability of traveling crossflow modes alone is studied herein to obtain useful insights regarding their breakdown. Results presented in a previous paper[16] showed that the traveling crossflow modes saturate at much lower amplitudes in comparison to the stationary modes and, yet, the growth of secondary instabilities of the traveling crossflow vortices can be at least as strong as those of the stationary crossflow modes. The work presented herein extends that effort to address the important issue of what threshold initial amplitudes are required for the traveling vortices to sustain a significant amplification of secondary instabilities.

Additionally, the predictions based on the secondary instability theory are compared with direct numerical simulations (DNS) with controlled initial disturbances.

The paper is organized as follows. Section II provides a brief background on the secondary instability theory for traveling crossflow instabilities in a swept wing boundary layer. For a more complete description of underlying methodology, the reader is referred to Refs. 18 and 19. The flow configuration of interest in this paper is outlined in Sec. III, along with the computational codes used in the analysis. The computational results are discussed in Sec. IV, followed by concluding remarks in Sec. V.

II. SECONDARY INSTABILITY

Secondary instability is an instability mechanism of the primary instability. Examples of primary instabilities in swept wing boundary layers include Tollmien-Schlichting waves, Görtler vortices, and crossflow vortices. The initial growth of a primary instability of infinitesimal amplitude is usually exponential and, as the amplitude increases downstream, nonlinear effects often lead to a quasi-saturation behavior. In strictly parallel flows such as a plane Poiseuille flow, the primary amplitude reaches a finite constant value. In many other cases such as external boundary-layer flows, however, the primary wave amplitude continues to evolve slowly as a result of the slow streamwise variations in the base flow.

The quasi-saturated, finite amplitude primary wave can become susceptible to an instability of its own, namely, the secondary instability.[20] Many examples of primary waves are time-independent when viewed in a proper inertial frame of reference and are periodic in at least one spatial direction. When the boundary layer flow is invariant along a spatial direction such as the spanwise direction in the case of a two-dimensional or infinite-span swept wing, the modified basic state in the presence of stationary Görtler or crossflow vortex modes is periodic in the spanwise direction and time-independent in a fixed frame of reference. Traveling crossflow vortices in such boundary layers are also periodic in the spanwise direction and appear stationary when the observer travels with the spanwise phase velocity of the vortex modes.

A local secondary instability analysis becomes possible when the slowly varying base flow is approximated as locally constant along the direction of slow mean flow evolution, because the coefficients of the perturbation equation become locally independent of that direction. The stationary and periodic nature of the primary waves greatly facilitates the analysis of secondary instabilities. If the flow field with a saturated primary wave is used as the base flow on which an infinitesimal perturbation is introduced, then the resulting linearized equations governing the evolution of the perturbation take the form of a set of linear partial differential equations with periodic coefficients in one of the directions. For Görtler and crossflow vortices, the periodic direction is along the wing span.

When the primary instability corresponds to crossflow vortices, the base flow is slowly varying along the vortex axis but periodic in the spanwise direction with the same period as the spanwise wavelength of the primary crossflow vortex. These two directions are, in general, not orthogonal and the problem is best solved in a non-orthogonal coordinate system. The derivation of secondary instability equations is described by Li and Choudhari,[19] who described the development of a self-consistent spatial formulation of secondary stability theory for infinite-span swept wing boundary layers. The spatial theory extended the simpler, temporal formulation described in the preceding incompressible studies by Malik *et al.*,[2] which provides the expressions for the coefficients for the 2D partial-differential-equation based eigenvalue problem for incompressible flow in Eqs. (5.2)–(5.5) of Ref. 2. A similar process was followed by Li and Choudhari[18,19] in generating the compressible equivalents of the coefficient matrices for an orthogonal system by symbolic manipulation software. These coefficients were then transformed into the non-orthogonal system of Eq. (1) below as described in Eqs. (4) and (5) of Li and Choudhari.[19] The secondary instability equations in a non-orthogonal coordinate system take the form,

$$\Gamma \frac{\partial \phi}{\partial t} + A \frac{\partial \phi}{\partial \xi} + B \frac{\partial \phi}{\partial \eta} + A \frac{\partial \phi}{\partial \zeta} = V_{\xi\xi} \frac{\partial^2 \phi}{\partial \xi^2} + V_{\eta\eta} \frac{\partial^2 \phi}{\partial \eta^2} + V_{\zeta\zeta} \frac{\partial^2 \phi}{\partial \zeta^2} + V_{\xi\eta} \frac{\partial^2 \phi}{\partial \xi \partial \eta}$$
$$+ V_{\eta\zeta} \frac{\partial^2 \phi}{\partial \eta \partial \zeta} + V_{\xi\zeta} \frac{\partial^2 \phi}{\partial \xi \partial \zeta}, \tag{1}$$

where $\phi(\xi, \eta, \zeta)$ is a vector representing perturbation quantities of secondary instability, ξ is the coordinate along the crossflow vortex axis, η is normal to the wall, and ζ is the spanwise coordinate. The coefficient matrices in front of the derivatives of ϕ are functions of the coordinates (ξ, η, ζ), slow-varying in ξ and periodic in ζ. The perturbation variables associated with the secondary instability can then be expressed in the form

$$\phi(\xi, \eta, \zeta) = \varphi(\eta, \zeta; \xi) \exp(-i\omega_s t + i\alpha\xi), \tag{2}$$

where $\varphi(\eta, \zeta; \xi)$ is a 2D complex function corresponding to the mode shape of secondary instability at station ξ along the axis of the primary crossflow vortex (i.e., the ξ dependence of φ is treated in a parametric sense), ω_s is the angular frequency of the secondary instability (treated as a real parameter in predicting the spatial evolution of secondary instability) and α is the complex wavenumber in the direction of the primary crossflow vortex. After substituting the modal ansatz (2) into the governing equations (1), the resulting set of equations is given by

$$-i\omega_s \Gamma\varphi + (i\alpha A + \alpha^2 V_{\xi\xi})\varphi + (B - i\alpha V_{\xi\eta})\frac{\partial\varphi}{\partial\eta} + (C - i\alpha V_{\xi\zeta})\frac{\partial\varphi}{\partial\zeta}$$

$$= V_{\eta\eta}\frac{\partial^2\varphi}{\partial\eta^2} + V_{\zeta\zeta}\frac{\partial^2\varphi}{\partial\zeta^2} + V_{\eta\zeta}\frac{\partial^2\varphi}{\partial\eta\partial\zeta}. \tag{3}$$

Together with appropriate boundary conditions in η and ζ directions, the equation set (3) corresponds to a 2D, i.e., planar, partial differential equation based eigenvalue problem. Equation (3) has coefficients that are 1-periodic in ζ (where the notation n-periodic denotes periodic functions with a fundamental wavelength of n times the corresponding wavelength of the primary crossflow mode), but its solution is not necessarily periodic in ζ. It takes the following form given by the well-known Floquet theory:[20]

$$\varphi(\eta, \zeta) = \Phi(\eta, \zeta)\exp(\frac{i\varepsilon\beta\zeta}{2}), \tag{4}$$

where Φ is 1-periodic in ζ, β is the spanwise fundamental wavenumber of the crossflow vortex and, in general, ε is a complex number that will be referred to herein as the detuning parameter. If the solutions to Eq. (3) are restricted to periodic functions of ζ, then ε becomes a real parameter. In particular, φ is 1-periodic when $\varepsilon = 0$ and 2-periodic when $\varepsilon = 1$, which correspond to the fundamental and subharmonic modes, respectively, of the secondary instability. In this paper, however, we are primarily interested in the fundamental modes. Computations of subharmonic modes at selected frequencies show that such modes do not behave very differently from their fundamental counterparts other than a 180° phase shift between the locations of peak oscillations across a pair of adjacent crossflow vortex modes. It may be noted that, once a solution is obtained in the non-orthogonal coordinate system (ξ, η, ζ), it can be easily remapped to the more intuitive orthogonal system (X, Y, Z), where Y and Z are in the same directions as η (wall-normal) and ζ (spanwise), respectively, and X is the surface coordinate normal to the leading edge of the wing.

For traveling crossflow vortices, the base flow (i.e., boundary layer flow plus the finite amplitude traveling crossflow perturbations) itself is unsteady. To circumvent the temporal variations in the base flow, the problem is analyzed in an inertial frame of reference traveling with the spanwise phase velocity of the crossflow vortex, which makes the base flow in the traveling frame independent of time as described by Malik *et al.*[21] The transformation from the stationary to traveling coordinate system is given by

$$\bar{Z} = Z - \omega_p t/\beta, \tag{5}$$

where $\bar{Z}$ is the spanwise coordinate in traveling system and ω_p is the fundamental frequency of the crossflow vortex in the fixed system. The stationary base flow in the traveling frame of reference can be expressed in the form

$$\bar{\phi}(x, y, \bar{Z}) = \sum_{n=-\infty}^{\infty} \hat{\bar{\phi}}_n(x, y)\exp(in\beta\bar{Z}). \tag{6}$$

Secondary instability analysis in this traveling coordinate system is very similar to the secondary instability of a stationary crossflow mode, except that the base flow spanwise velocity is now non-zero at the wall. In the spanwise traveling frame, each linear secondary instability mode can be associated with a single fixed angular frequency, ω_s. Just as for the secondary instability of stationary crossflow modes,[18,19] the secondary instability of traveling crossflow modes can be expressed in terms of the Fourier series expansion

$$\phi\left(x, y, \bar{Z}, t\right) = \sum_{n=-\infty}^{\infty} \hat{\phi}_n\left(x, y\right) \exp\left(in\beta\,\bar{Z} - i\omega_s t\right). \tag{7}$$

In experiments, the measurement devices are usually fixed in the stationary frame of the wind tunnel. It is then natural to inquire what frequency or frequencies would be registered by the measurement sensors? This question can be answered by substituting Eq. (5) into Eq. (7) to obtain the expression for the secondary perturbation in the fixed frame of reference:

$$\phi\left(x, y, Z, t\right) = \sum_{n=-\infty}^{\infty} \hat{\phi}_n\left(x, y\right) \exp\left(in\beta Z - (in\omega_p + i\omega_s)t\right), \tag{8}$$

whereas the base flow in this fixed frame of reference is given by

$$\bar{\phi}\left(x, y, Z, t\right) = \sum_{n=-\infty}^{\infty} \hat{\bar{\phi}}_n\left(x, y\right) \exp\left(in\beta Z - n\omega_p t\right). \tag{9}$$

In practice, the frequency of secondary instability is often an order of magnitude higher than that of the primary wave, i.e., $\omega_s \gg \omega_p$, it is convenient, for illustrative purpose, to consider a secondary instability of a frequency that is an integer multiple of the primary wave frequency. Let such a fixed integer be denoted by, k, then Eq. (8) becomes

$$\phi\left(x, y, Z, t\right) = \sum_{n=-\infty}^{\infty} \hat{\phi}_n\left(x, y\right) \exp\left(in\beta Z - i(n + k)\,\omega_p t\right). \tag{10}$$

Let us now consider the structure of both the base flow and the secondary fluctuations in the discrete Fourier space (m, n), where m denotes the temporal harmonic and n represents the spanwise harmonic. In the spanwise traveling frame, the base flow is spread over the vertical axis corresponding to Fourier modes $(0, n)$ and the secondary instability mode is spread over the parallel line corresponding to Fourier modes $(1, n)$. In a fixed frame of reference, on the other hand, the same two fields occupy the diagonal lines corresponding to Fourier modes (n, n) and $(n + k, n)$, respectively. Consequently, when the primary instability corresponds to traveling crossflow modes, a linear secondary instability mode in the fixed frame of reference is characterized by multiple frequencies that overlap with the frequency range of the nonlinear primary mode. Therefore, in practice, a fixed probe may not be able to distinguish the contributions of the secondary instability from those of the primary instabilities within the Fourier space. Figure 1(a) illustrates the locations of the primary and secondary modes with distinct frequencies in the discrete Fourier space in the traveling frame of reference. Figure 1(b) shows the corresponding locations in a fixed frame of reference for an illustrative case with $k = 9$, wherein the overlap in frequencies within the fixed frame is easily observed. We note that the above discussion is purely for illustrative purpose. In our subsequent computations, there is no assumption about the ratio of ω_s and ω_p. Because of the moving frame of reference in which our computations are carried out, the primary traveling crossflow vortices appear to have 0 frequency and as a result, the secondary instability modes of any frequency can be set as the fundamental unsteady mode $(m = 1)$ in the discrete Fourier space without unduly stretching the computational resources.
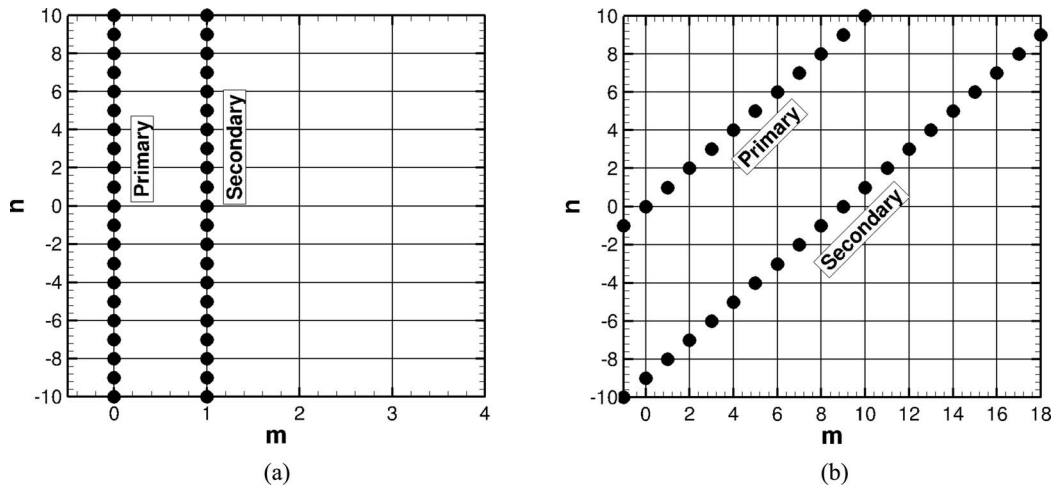
FIG. 1. Schematic of primary and secondary modes in discrete Fourier space. (a) In traveling frame of reference, primary and secondary modes have distinct frequencies. (b) In fixed frame of reference ($k = 9$), primary and secondary modes have overlapping frequencies.

The equation set (3) for the secondary instability is subject to boundary conditions of vanishing perturbation quantities at the wall and freestream boundaries. The spanwise boundary conditions are not explicitly specified, as they are automatically imposed as part of the admissible solutions given by Eq. (4). The main difference between a stability equation governing the secondary instability and that governing the primary instability is that the coefficients of the secondary modes are functions of two spatial variables instead of just one for the case of the primary modes. Thus, the resulting eigenvalue problem is also referred to as a 2D eigenvalue problem.[22]

III. FLOW CONFIGURATION AND ANALYSIS CODES

The flow configuration employed in the present study corresponds to the laminar flow airfoil TAMU-003T-75(v.90), which is described in detail by Belisle *et al.*[23] The 9.3% thick, 30° swept wing is designed to achieve natural laminar flow over approximately 60% and 50% of the suction and pressure surfaces, respectively, at the design condition of $M = 0.75$, AoA = 0°, and $Re_c \approx 17 \times 10^6$. Here, the non-dimensional parameters M and Re_c are based on the freestream speed, a streamwise chord length of 12 ft, and a freestream temperature of 390° R, corresponding to a flight altitude of 40 000 ft. Design constraints for the wing included (i) lift coefficients that are typical of subsonic transports, e.g., 0.37 and 0.49 at AOAs of 0° and 1°, respectively and (ii) a wing thickness distribution that is suitable for a mid-size business jet. Both Tollmien-Schlichting and crossflow instabilities are sufficiently weak at the design angle of attack, so that natural laminar flow should be achievable over a significant portion of the wing surface on both suction ($0 < X/C < 0.6$) and pressure ($0 < X/C < 0.5$) sides without any external means of boundary layer control. In the present research, we focus on the off design condition corresponding to an angle of incidence equal to $-1°$. At this condition, an even stronger crossflow instability than the design condition is known to exist along the suction side.[23]

For the present work, the mean boundary-layer flow over the suction surface of the wing is computed with a boundary layer solver[24] by using the infinite span approximation, in conjunction with the inviscid surface pressure distribution derived from an Euler solution under free flight conditions.[25] Linear and nonlinear development of the instability modes is computed using parabolized stability equations (PSE) as implemented in the Langley Stability and Transition Analysis Codes (LASTRAC).[26] The growth of high frequency secondary instability modes supported by the finite amplitude stationary crossflow vortex is analyzed in a manner similar to the classical linear stability analysis of swept wing boundary layers. Details of the computational methodology employed for linear secondary instability analysis (LSIT) may be obtained from Refs. 18 and 19, and

the essential modifications for the traveling mode case are mentioned in Ref. 16 and Sec. II. DNS computations are also carried out for both finite amplitude traveling crossflow vortices and their secondary instability. Details of the DNS method used in the analysis can be found in Refs. 27 and 28. The main difference between the primary and secondary stability analyses is that the basic state for the secondary modes (i.e., the mean boundary layer flow modified by the primary crossflow mode) varies in both surface normal and spanwise directions and, hence, the instability characteristics of the secondary modes must be analyzed using a planar, partial differential equation based eigenvalue problem, rather than as an ordinary differential equation based eigenvalue problem for the classical analysis. The selection of grid and other aspects of the numerical solution were based on extensive experience with similar class of flows[3, 16, 19, 29–33] and checks were made to ensure that the impact of variations with respect to those choices was negligible.

For 2D eigenvalue problems corresponding to linear secondary instability, 121 and 32 grid points are usually used in the wall-normal and spanwise directions, respectively. For NPSE computations of a typical nonlinear primary wave (i.e., the traveling crossflow vortex) in the traveling frame of reference, the number of spanwise Fourier modes used is 50, i.e., n ranging from -50 to 50, and the number of grid points in the wall-normal direction is 281. In addition, for monitoring the development of secondary instability using NPSE, 5 Fourier modes are used to resolve the time evolution, i.e., m ranges from -5 to 5. Previous experiences with and tests on similar problems[18, 19, 31, 32] show that the grid resolutions described above are sufficient to resolve all relevant scales up to the transition location for the problems at hand.

The DNS computations are based on a grid of size $2184 \times 60 \times 418$ points in streamwise, spanwise, and wall-normal directions, respectively. An additional set of DNS computations was performed using a grid that was 1.5 times coarser in both spanwise and wall-normal directions. The amplitude evolution based on the coarser grid agreed well with the fine grid solution presented here, except for weak streamwise oscillations in the region downstream of the main lobe in instability growth rate as a function of *X/C*. The streamwise resolution of the DNS grid corresponds to a minimum of 40 points per fundamental wavelength.

IV. RESULTS

The computational results for the nonlinear development of traveling crossflow vortices and the associated linear growths of secondary instabilities are presented in Subsections IV A and IV B.

A. Nonlinear evolution of a traveling crossflow mode

A comparison of the nonlinear amplification characteristics for stationary and traveling crossflow modes with a fixed spanwise wavelength of $\lambda_z = 8$ mm was presented in Ref. 16. That analysis is expanded herein by considering a broader range of spanwise wavelengths. To allow selection of the most relevant frequency-wavenumber combinations for these nonlinear calculations, linear N-factor computations for the traveling crossflow instability were carried out with linear PSE. As a reminder to the reader, the N-factor of a disturbance at a specific chordwise location is defined as the integral of the disturbance growth rate from its neutral point to that location. This selection process is based on the same premise as the N-factor method for transition prediction, namely that transition is likely to be caused by the instability mode that first achieves a linear amplification ratio corresponding to a specified value of N. This mode may or may not correspond to the mode that achieves the highest overall N-factor over the wing chord. Based on the aforementioned criterion, traveling crossflow instability modes with spanwise wavelengths of 6, 8, and 10 mm and a frequency of 1500 Hz were found to reach N = 10 before most other traveling modes and, hence, were selected for nonlinear analysis in this paper. For $\lambda_z = 12$ mm, the mode with a lower frequency of 1225 Hz reaches N = 10 first; however, its N-factor value of 10 is only slightly higher than that of the traveling crossflow mode with a 1500 Hz mode. Therefore, to enable consistent comparisons across different wavelengths, the 1500 Hz mode is analyzed in this paper even for the $\lambda_z = 12$ mm wave.

Figure 2(a) shows the linear N-factor curves for crossflow instability modes with $\lambda_z = 8$ mm for selected frequencies ranging from 0 to 2250 Hz. As expected, the most amplified traveling mode
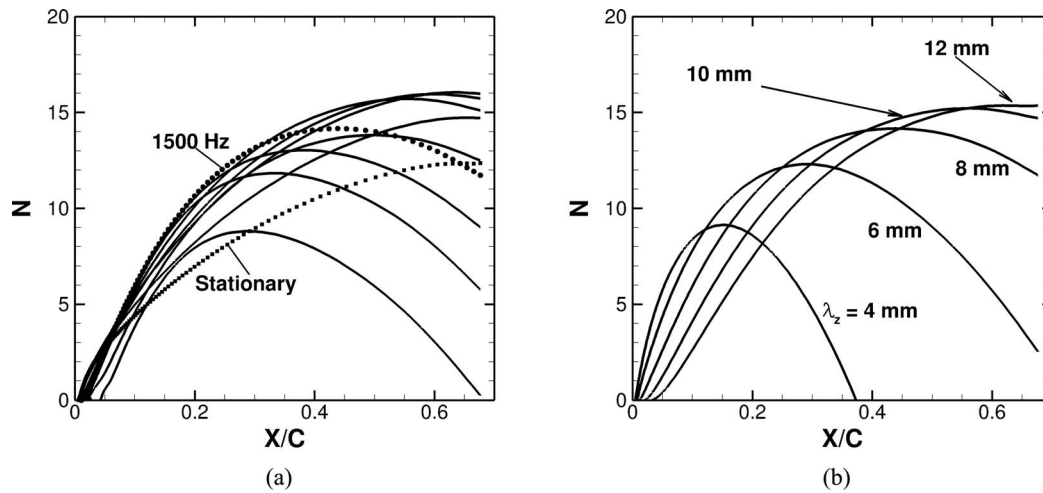
FIG. 2. Linear N-factors for crossflow instability. (a) Crossflow instability modes with $\lambda_z = 8$ mm and frequency ranging from 0 to 2.25 kHz. The N-factor first reaches a value of 10 for the 1500 Hz. (b) Linear N-factors for various spanwise wavelengths at a frequency of 1.5 kHz.

achieves higher N-factors than the stationary mode and, more importantly, the traveling mode with $f = 1500$ Hz reaches N = 10 within nearly half the distance it takes for the stationary crossflow mode ($f = 0$) to reach the same N-factor value. This indicates the need to study the breakdown of traveling waves to obtain a more complete picture of crossflow-dominated transition, especially when the relative initial amplitudes of the traveling crossflow modes are not sufficiently small in comparison with those of the stationary modes.

Figure 2(b) shows N-factor curves for various spanwise wavelengths at 1500 Hz; and the $\lambda_z = 6$ mm wave reaches an N-factor of 10 before the longer waves, even though the overall maximum N-factor is reached by the 12 mm mode.

The amplitude of the perturbation becomes an important parameter in a nonlinear framework. Throughout the present work, the non-dimensional amplitude of a perturbation is defined as the ratio of the peak chordwise perturbation velocity to the freestream speed, i.e., the perturbation velocity as a fraction of the freestream speed. Comparisons between nonlinear developments of traveling and stationary vortices were presented by Choudhari *et al.*[16] Since this is an important component of this analysis, showing characteristic differences between the two types of crossflow vortices, the essential results are reproduced here. Figure 3(a) shows comparisons of the nonlinear development of stationary and traveling crossflow vortices of the same spanwise wavelength ($\lambda_z = 8$ mm) and the same initial amplitude ($A_{init} = 1 \times 10^{-5}$). This particular spanwise wave length was chosen because the linear and nonlinear PSE computations by Li *et al.*[31, 32] had indicated the crossflow vortex with $\lambda_z = 8$ mm to be one of the most likely stationary modes to cause transition. The essential results of Ref. 16 are that the traveling crossflow vortices saturate at lower fundamental amplitudes than the stationary vortices, approximately just one half of the saturation amplitude of the latter, while the peak mean flow correction amplitudes for both stationary and traveling modes reach comparable levels. This comparison between the nonlinear evolution of isolated traveling and stationary crossflow disturbances is very similar to that reported by Malik *et al.*[33] for a different wing configuration and to that by Wassermann and Kloker[15] for a flat plate subject to a favorable pressure gradient. Therefore, these findings appear to be more general and not restricted to just one specific case.

Modal amplitudes of traveling crossflow vortices of 1500 Hz analyzed in Ref. 16 are shown in Figure 3(b) for initial amplitudes of 2.5×10^{-6}, 5.0×10^{-6}, 7.5×10^{-6}, and 10^{-5}. Amplitudes of the mean flow correction and the first harmonic are also shown for the case of the smallest initial amplitude. The general features of oscillatory behavior and decay after saturation as seen earlier in Figure 3(a) for $A_{init} = 1 \times 10^{-5}$ are present for all initial amplitudes, with waves corresponding to higher initial amplitudes exhibiting an earlier quasi-saturation. Figure 3(b) also indicates
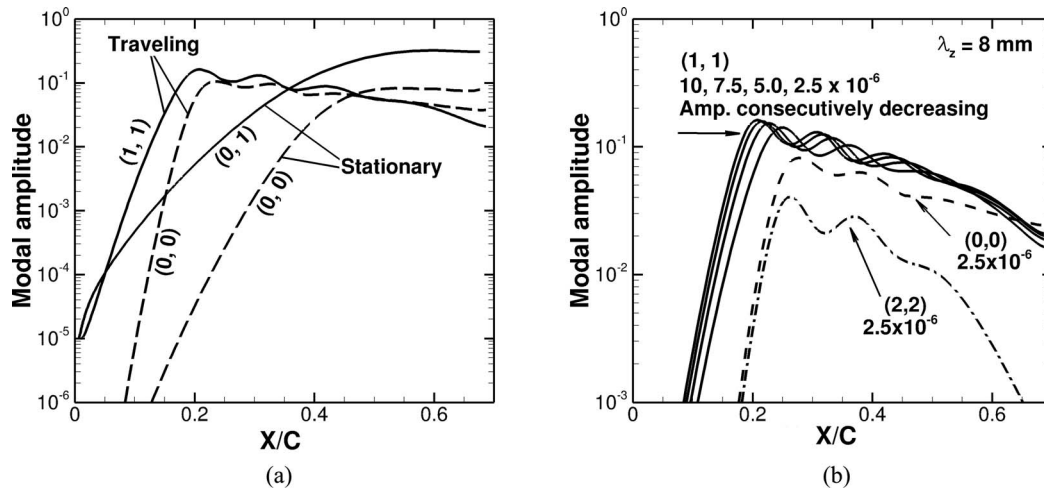
FIG. 3. Nonlinear evolution of crossflow vortex modal amplitudes (Ref. 16). (a) Stationary and traveling crossflow (f = 1.5 kHz) modes with $\lambda_z = 8$ mm and the same initial amplitude ($A_{init} = 1 \times 10^{-5}$): Comparison of modal amplitudes for the fundamental and mean flow correction modes. (b) Fundamental mode amplitude for 8 mm traveling crossflow vortices with different initial amplitudes. The amplitudes of mean flow correction and the first harmonic are also shown for the case with the smallest initial amplitude ($A_{init} = 2.5 \times 10^{-6}$).

that traveling crossflow modes with higher initial amplitudes saturate at progressively larger peak amplitudes.

Now the nonlinear analysis is expanded to a range of other wavelengths. Figure 4(a) shows the nonlinear evolution of traveling crossflow vortices with $f = 1500$ Hz and $\lambda_z = 6, 8, 10,$ and 12 mm, respectively. The number of spanwise Fourier modes retained is 50 in the NPSE computations, which is more than necessary to resolve the spanwise variations of the crossflow vortex. The initial amplitudes, defined as the chordwise perturbation velocity as a fraction of the freestream velocity, for all spanwise wavelengths are held fixed at 10^{-5}. As expected from the results of linear computations discussed earlier, the 6 mm wave rises in amplitude first and is followed by waves of consecutively larger wavelengths. The highest overall amplitude is reached by the 8 mm wave, and not the 12 mm wave corresponding to the highest value of linear N-factor. Due to nonlinear effects, the 12 mm wave saturates at a lower peak amplitude than the 8 mm wave. However, the hierarchy based on peak fundamental mode amplitudes is dependent on the initial amplitude of the wave. In particular, when the initial amplitude is lowered to 2.5×10^{-7}, the $\lambda_z = 10$ mm mode has the highest peak amplitude as shown in Figure 4(b). As the initial amplitude is further lowered, the nonlinear effects become rather weak; and hence, the 12 mm wave becomes dominant as predicted by the linear theory (Figure 4(c)).

The results in Figure 4 also show that, in all cases with a significant effect of nonlinearity (i.e., for sufficiently large initial amplitudes), the amplitude of the fundamental mode evolves in an oscillatory manner. The initial evolution up to the first peak is strictly monotonic; and in general, this first peak also represents the global maximum of the fundamental mode amplitude. However, the subsequent evolution of the fundamental amplitude displays oscillatory behavior superimposed on a decaying trend. Gajjar[34] observed similar oscillations in a theoretical study of stationary crossflow vortices. The oscillations are believed to have been caused by the interaction of the fundamental and mean flow correction modes. Figure 4(d) shows the evolutions of the fundamental and mean flow correction modes for the 1500 Hz, 10 mm traveling wave with initial amplitude of 10^{-5}. Their respective oscillations appear to be approximately $90°$ out of phase. The fundamental mode, of course, initially drives up the mean flow correction. When it becomes sufficiently large, the mean flow correction mode modifies the boundary layer in such a way that the fundamental mode is stabilized and its amplitude starts to drop. As the mean flow correction mode reaches its peak, the rate of decay of the fundamental mode is approximately the largest. Further drop in the fundamental amplitude, in turn, leads to a decrease in the mean flow correction amplitude, which causes the fundamental mode to grow again. And this interactive process repeats itself downstream. An NPSE
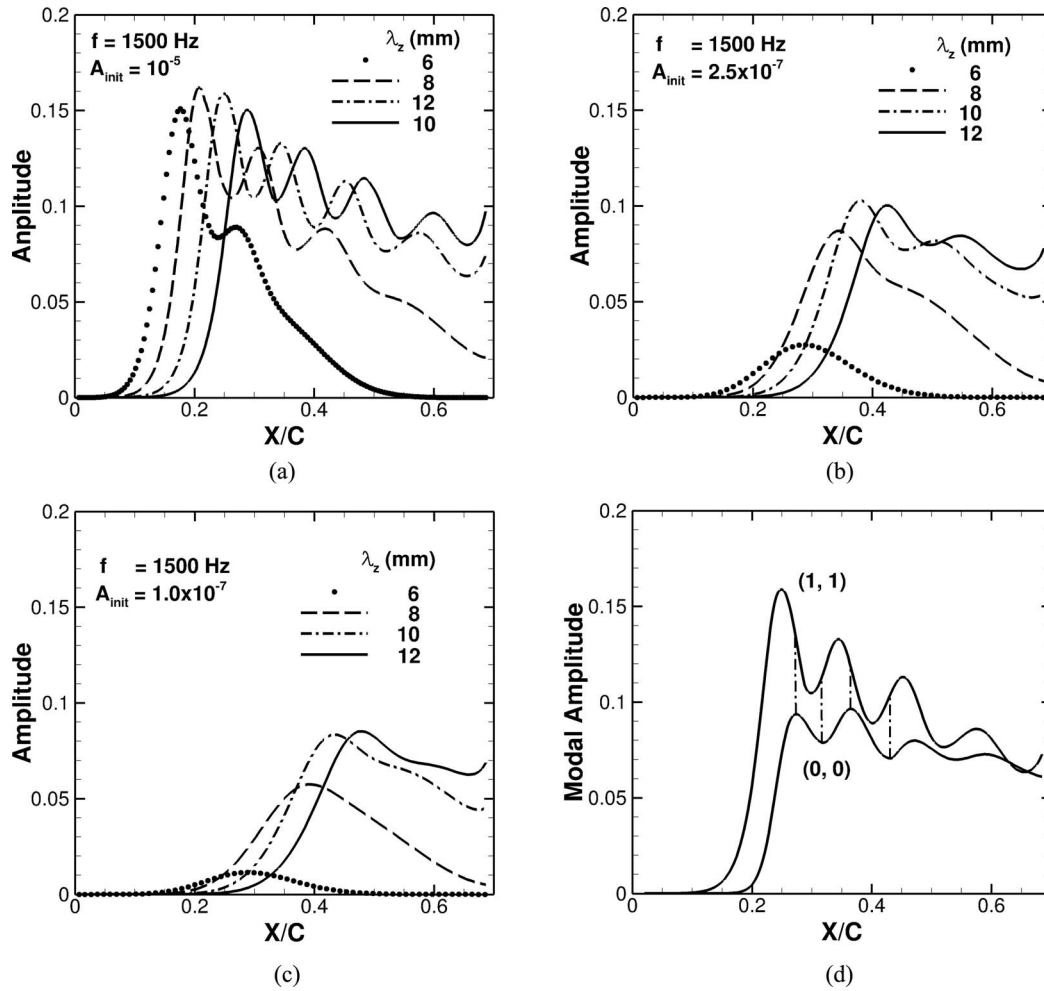
FIG. 4. Evolution of modal amplitudes. (a) Fundamental mode amplitude. $f = 1.5$ kHz, $A_{init} = 10^{-5}$. (b) Fundamental mode amplitudes. $f = 1.5$ kHz, $A_{init} = 2.5 \times 10^{-7}$. (c) Fundamental mode amplitudes. $f = 1.5$ kHz, $A_{init} = 1 \times 10^{-7}$. (d) Fundamental and mean flow correction modes with approximately $90°$ phase difference. Vertical dashed-dotted lines indicate corresponding locations of peak meanflow correction and rapid rate of change of fundamental mode. $A_{init} = 10^{-5}$, $\lambda_z = 10$ mm, $f = 1.5$ kHz.

computation with only the fundamental and the mean flow correction terms retained reproduces exactly the same oscillatory behavior. Additionally, an NPSE computation with one more Fourier mode retained, namely the first harmonic, also produces very similar result with some modifications in modal amplitudes only, indicating that the first harmonic is not an active player in the interactive process. This confirms that the interaction of two modes and these two modes alone is responsible for the oscillations.

To help validate the PSE predictions for nonlinear evolution of the primary, traveling crossflow instabilities, DNS computations were also carried out for 1,500 Hz modes in the traveling frame of reference discussed in Sec. II. The DNS solutions are based on a spatial grid of size $981 \times 40 \times 278$ in the streamwise, spanwise, and wall-normal directions, respectively. Following Jiang *et al.*,[35] the *i*-coordinate of the grid is aligned with the constant phase surfaces of the traveling crossflow vortex to reduce the number of points required to resolve the wavy structure of the mode in the chordwise direction. To further save on the computational resources, the chordwise extent of the domain is restricted by choosing an inflow location at $X/C = 0.15$, i.e., somewhat farther downstream from the lower branch neutral station domain at $X/C \approx 0.05$. The linear eigenfunction of the 1500 Hz traveling mode is imposed at the inflow with an initial amplitude that is equivalent to $A_{init} = 5 \times 10^{-7}$.
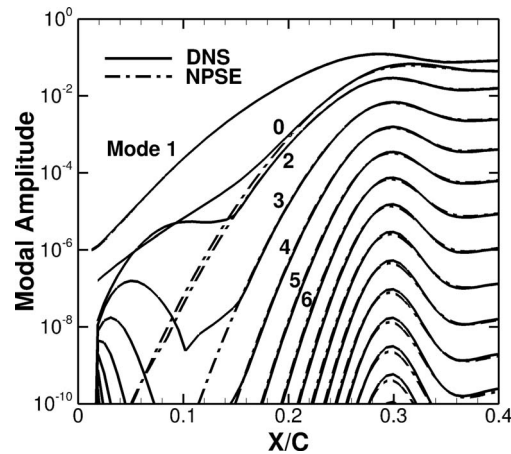
FIG. 5. Evolution of modal amplitudes for traveling crossflow vortices with initial amplitude of 5×10^{-7}. Comparison between results of nonlinear PSE and direct numerical simulations. Solid lines and dash-dot lines represent results of DNS and NPSE computations, respectively.

The DNS results are compared with the NPSE results in Figure 5 with m denoting the harmonic index, i.e, when the frequency of the fundamental mode is 1500 Hz, the m'th mode has a frequency of $1500 \times m$ Hz. At the inflow location, the NPSE result shows that only the fundamental mode is present and subsequently, the mean flow correction mode ($m = 0$) and other harmonic modes ($m > 1$) are driven up due to nonlinear interactions between modes. These modes behave in a similar way as those in stationary crossflow vortices. The mean flow correction mode ($m = 0$) and the second harmonic mode ($m = 2$) are, initially, the dominant driven modes and have comparable amplitudes because they are both generated by self-interactions of the fundamental mode. Higher harmonics that are forced by hetero-interactions of mode shave consecutively smaller amplitudes. Eventually, the nonlinearly developed disturbance appears to saturate. The amplitude evolution of the fundamental mode ($m = 1$) from DNS compares very well with that from NPSE right from the beginning of the DNS domain. This is not the case for the mean flow correction mode and the higher harmonics. For DNS, these modes undergo a transient phase, but eventually settle to match the results of NPSE.

B. Secondary instability of traveling crossflow vortex

In this subsection, the secondary instability of traveling crossflow vortices is analyzed and comparisons among of LSIT, NPSE and DNS results are presented.

1. Linear amplification characteristics for primary waves of selected frequency-wavelength combinations

The presence of crossflow vortices creates strong localized shear layers within the boundary layer. Secondary instability modes riding on crossflow vortices can be classified into two major types:[2] secondary modes associated with the strong wall-normal shear of the modified basic state are known as Y modes and those associated with a strong spanwise shear are known as Z modes. At times, when mean shears in both directions have comparable contributions to the energy production mechanisms associated with the secondary instability, the resulting modes have a mixed character and, hence, are termed as Y/Z modes.[16] The secondary instability of the non-stationary crossflow vortex with $\lambda_z = 8$ mm and $f = 1500$ Hz was discussed in Ref. 16. Here, a larger number of cases with different primary wave initial amplitudes and wavelengths are analyzed to help characterize the range of initial amplitudes below which the secondary instability of traveling crossflow modes becomes relatively insignificant in comparison with the secondary instability of stationary crossflow vortices.

The comparison of secondary instability growths on stationary and traveling crossflow vortices of the same initial amplitude was given in Ref. 16. The main result is reproduced in Figure 6 for
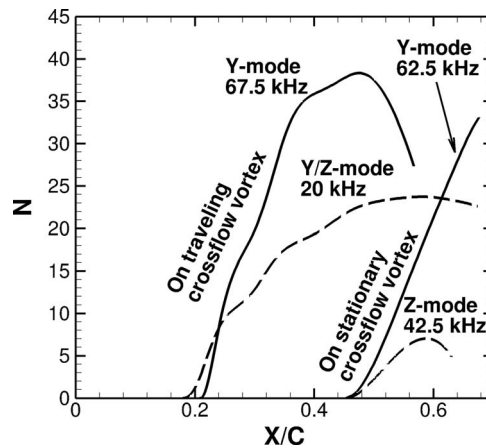
FIG. 6. Comparison of N-factor curves for most dangerous secondary instability modes of stationary and traveling crossflow vortices. The metric for growth potential corresponds to earliest attainment of N = 10, or of the highest N-factor if N = 10 is never achieved. Both stationary and traveling crossflow vortices have the same spanwise wavelength of 8 mm and the traveling mode has a frequency of 1500 Hz (Ref. 16).

an initial primary amplitude of 10^{-5}. The traveling crossflow vortex is seen to sustain secondary instability N-factors just as large as those for stationary waves even though the saturation primary amplitude of the traveling wave is only about one half that of the peak amplitude of stationary mode (see Figure 3(a)).

The onset of secondary instability is dependent on the primary wave amplitudes exceeding a threshold level that depends on both the local mean flow and the disturbance parameters. To help characterize the threshold amplitudes required for significant amplification of secondary instabilities, a parametric study is carried out for secondary instability modes for various initial amplitudes of the primary wave. Figure 7(a) shows the N-factor curves for secondary instability modes that first achieve an N-factor of 10 for each initial amplitude of the traveling crossflow vortex ranging from $A_{init} = 1.5 \times 10^{-7}$ to 10^{-5}. The wavelength ($\lambda_z = 8$ mm) and frequency ($f = 1500$ Hz) of the primary disturbance are the same in each of these cases. At relatively high initial amplitudes (approximately $A_{init} \geq 5 \times 10^{-6}$), the Y mode dominates. For example, for $A_{init} = 10^{-5}$, the peak N-factor reached by the Y mode is approximately 1.6 times the maximum N-factor achieved by the Y/Z mode. As the primary amplitude decreases, the maximum N-factors for both modes drop as expected. However, the Y-mode peak N-factor decreases faster with decreasing primary wave amplitude than the Y/Z-mode N-factor. At primary amplitude of 2.5×10^{-6}, the Y mode is approximately 13 and the Y/Z-mode N-factor has already overtaken the former with a peak value of 18. On further reduction of primary wave amplitude to 5×10^{-7}, no Y mode is picked up by the secondary instability analysis code, indicating that the Y-mode secondary instability has become substantially weaker. On the other hand, the Y/Z mode still reaches a peak N-factor of approximately 10.

The exact thresholds for the initial primary amplitude required for the onset of secondary instability cannot be defined without carrying out a systematic and time consuming set of computations over a broad range of primary wave amplitudes and streamwise locations. However, the data shown in Figure 7 reveals that the peak N-factor for the Y mode has reduced to less than 3.3 for $A_{init} \leq 10^{-6}$ and the peak N-factor of the Y/Z mode has fallen below 4.2 for $A_{init} \leq 1.5 \times 10^{-7}$. The corresponding peak amplitudes of the primary wave are approximately 12% and 7%, respectively. Thus, a conservative estimate is that, below these primary wave peak amplitudes, there is no significant secondary instability growth for the 8 mm traveling crossflow mode. For the Y modes shown in Figure 7, the peak frequency ranges from 58 to 67.5 kHz, and those for the Y/Z modes from 15 to 20 kHz.

A comparison is given next of the initial amplitudes of stationary and non-stationary crossflow modes required to reach N-factor values that are likely to correlate with transition. For a stationary crossflow mode of $\lambda_z = 8$ mm, the computations by Choudhari *et al.*[16] had shown that the initial primary amplitude required for a secondary instability mode on a traveling crossflow vortex to reach a
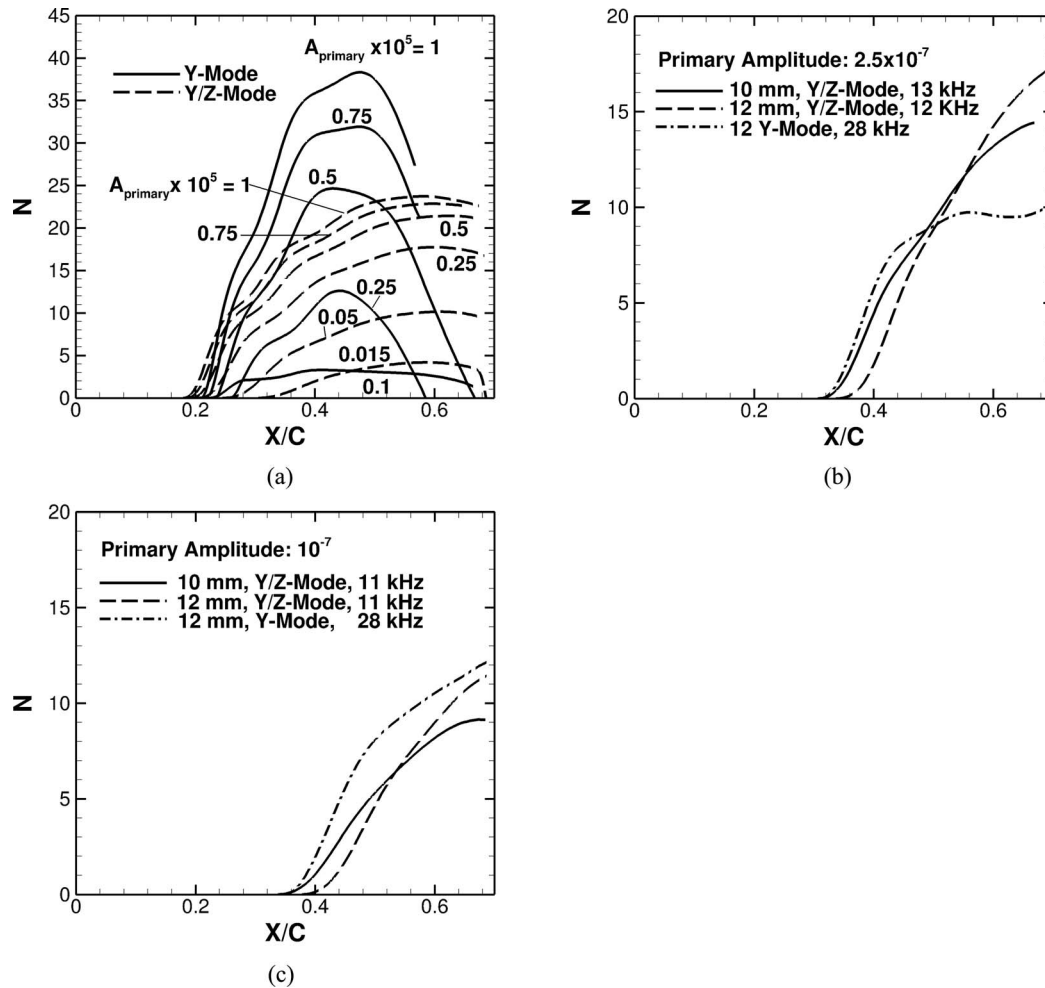
FIG. 7. Peak N-factors of secondary instability of traveling crossflow vortices. (a) Effect of different primary wave initial amplitudes, $\lambda_z = 8$ mm, (b) $\lambda_z = 10$ and 12 mm, $A_{init} = 2.5 \times 10^{-7}$. (c) $\lambda_z = 10$ and 12 mm, $A_{init} = 10^{-7}$.

given N-factor is much smaller than that required on a stationary crossflow vortex. Of course, because of the stronger receptivity mechanisms for stationary crossflow vortices,[36] the disparity between initial amplitudes of stationary and non-stationary crossflow modes is expected to be substantially greater in most low-amplitude environments. Thus, the next relevant question becomes how much smaller the traveling mode amplitudes need to be so that they do not play any significant role during the transition of the swept wing boundary layer. Based on the discussion of the threshold amplitudes in the preceding paragraph, this is predicted to happen for the $\lambda_z = 8$ mm traveling mode when its initial amplitude is more than one order of magnitude lower than the initial amplitude of the stationary crossflow mode. Of course, this conclusion only holds within the limited context of the present study; however, it provides useful guidance regarding the dominant mechanism for transition onset.

The secondary instability properties for primary waves of wavelengths other than $\lambda_z = 8$ mm are considered next. Recall from Figure 4 for $A_{init} \leq 2.5 \times 10^{-7}$ that the peak amplitude of 6 mm wave becomes small enough so that it is highly unlikely to sustain any significant secondary instability. On the other hand, the longer waves (10 and 12 mm) achieve large enough amplitudes to indicate the potential for significant secondary instabilities at farther downstream locations than the secondary instability modes of the $\lambda_z = 8$ mm wave. Therefore, secondary instability computations are carried out for the 10 and 12 mm waves for $A_{init} = 2.5 \times 10^{-7}$. The modes that achieve the highest N-factors in each case are plotted in Figure 7(b). For both wavelengths, strong Y/Z-mode secondary instability growth is found. In the case of the 12 mm wave, there is also a strong Y mode
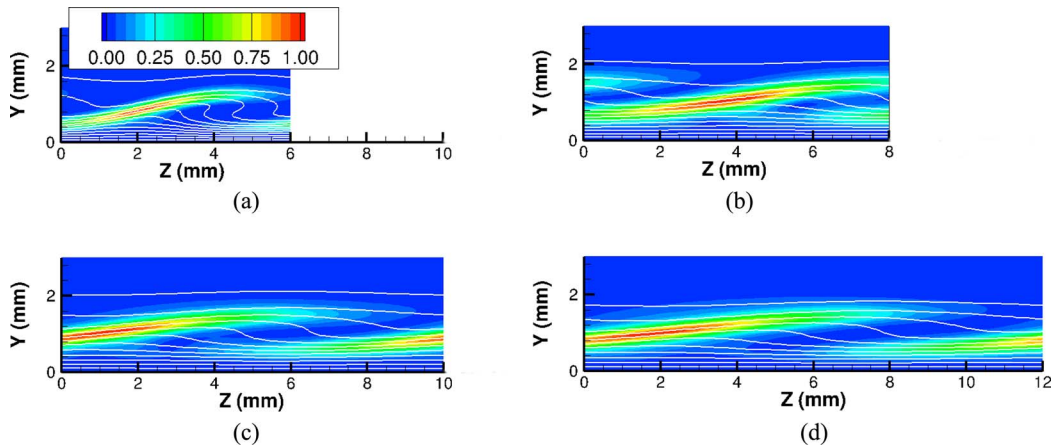
FIG. 8. Y/Z mode eigenfunctions (chordwise perturbation velocity) for secondary instability modes on primary waves with $f = 1500$ Hz and varying spanwise wavelength. Flood contours represent chordwise velocity perturbation associated with the secondary instability; white lines represent the base flow chordwise velocity. (a) $X/C = 0.18$, $\lambda_z = 6$ mm, (b) $X/C = 0.21$, $\lambda_z = 8$ mm, (c) $X/C = 0.38$, $\lambda_z = 10$ mm, and (d) $X/C = 0.43$, $\lambda_z = 12$ mm.

(Figure 7(b)). However, these Y modes attain an N-factor of 10 or greater significantly downstream of the mid-chord location, so that they would not be expected to play a role in transition even if the stationary crossflow modes were not a factor. Further reduction of their initial amplitudes pushes the large peak amplitudes downstream and hence delay, but not eliminate, the onset of secondary instability, as shown in Figure 7(c) for a primary amplitude of $A_{init} = 10^{-7}$. However, what can be said about the thresholds for secondary instability is that, for primary amplitudes below 2.5×10^{-7} and 10^{-7}, no N-factor greater than 3 is reached by any secondary instability mode before $X/C = 0.35$ and 0.4, respectively.

Figures 8(a)–8(d) show the Y/Z-mode eigenfunctions on primary waves with 1500 Hz in frequencies and 6, 8, 10, and 12 mm in spanwise wavelengths at chordwise locations where their respective fundamental amplitudes are largest. The primary waves for the 8, 10, and 12 mm cases all have the same initial amplitude of 2.5×10^{-7}. However, this amplitude is too small to sustain any secondary instability for the 6 mm primary wave, therefore, an initial amplitude of 1×10^{-5} is used instead for that case. These typical eigenfunction shapes are very similar to those found on stationary primary waves.[3]

Figure 9(a)–9(d) show the mean chordwise velocity contours of 1500 Hz crossflow instability waves in the traveling frame for spanwise wavelengths of 6, 8, 10, and 12 mm at the peak amplitude
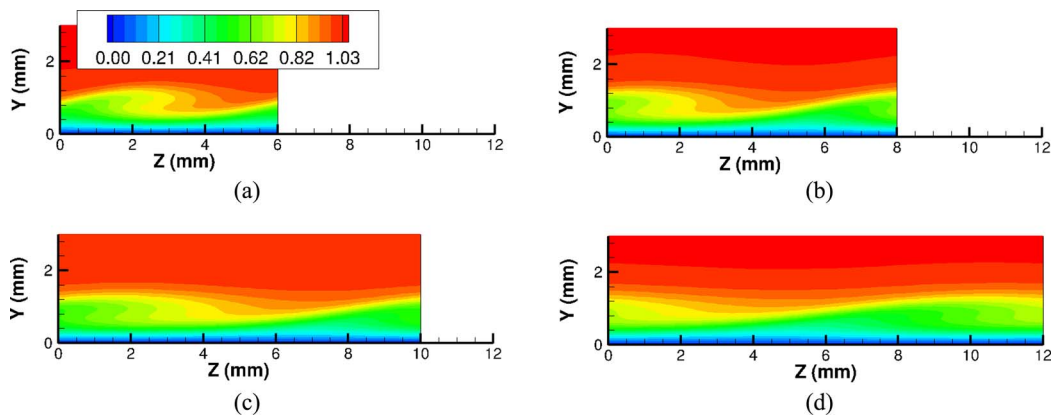

FIG. 9. Chordwise velocity (u/U_∞) contours associated with finite amplitude traveling crossflow modes of various spanwise wavelengths at chordwise location corresponding to the maximum wave amplitude in that case ($A_{init} = 10^{-5}$ in each case). (a) $X/C = 0.18$, $\lambda_z = 6$ mm, (b) $X/C = 0.21$, $\lambda_z = 8$ mm, (c) $X/C = 0.25$, $\lambda_z = 10$ mm, and (d) $X/C = 0.29$, $\lambda_z = 12$ mm.

streamwise locations, respectively, all with an initial amplitude of 10^{-5}. The shortest wave (6 mm) shows only a hint of the turnover feature that is almost ubiquitously present in stationary crossflow vortices, but the structure is not nearly as strong as in the latter case. As the spanwise wavelengths becomes longer, this feature diminishes and is hardly discernible for the longest 12 mm wave. This may be attributed to the relatively low saturation amplitude of the traveling crossflow vortex as discussed earlier.

2. Comparison of LSIT predictions with NPSE and DNS

Secondary instability computations using NPSE and DNS are also carried out for comparison with the secondary instability theory for the primary mode with $\lambda_z = 8$ mm, $f = 1{,}500$ Hz, and A_{init} $= 5 \times 10^{-7}$. Computations are performed for a fixed-frequency secondary instability mode with a frequency of 13.5 kHz, which is close to the most amplified Y/Z mode in this case. As discussed before, at the relatively low value of A_{init} for the primary crossflow vortex, the Y mode of secondary instability is nearly stable, but the Y/Z mode is still strong. Furthermore, in the experiments on stationary crossflow vortices,[37] the Y mode has been less commonly observed than the secondary instability modes associated with spanwise basic state shear. Therefore, a Y/Z mode is chosen for the DNS analysis. The linear eigenfunction of the 13.5 kHz secondary instability mode is imposed at a streamwise location of $X/C = 0.265$, i.e., slightly downstream of its neutral point. The minimum wavelength of this mode in the i-direction of the grid in the computational domain is approximately 12.7 mm.

Figure 10(a) shows the amplitude evolutions of the 13.5 kHz Y/Z-mode secondary instability as computed by three different methods, namely, LSIT, NPSE, and DNS. The comparison of NPSE and DNS results, while not perfect, is good. The LSIT method, however, is found to over-predict the instability growth downstream by a significant amount compared to the NPSE and DNS results. The differences that accumulate with distance may be attributed to the different degrees of approximations inherent to each of these methods. The LSIT method assumes a quasi-parallel base flow (i.e., slowly varying laminar boundary layer as well as traveling crossflow amplitude), which becomes less accurate when the base flow changes relatively rapidly, e.g., in regions of stronger growth or decay of the primary wave. The NPSE method takes into account the non-parallelism of the base flow, but assumes that streamwise second derivatives of perturbation amplitudes are negligible due to their slow variation in the streamwise direction. Furthermore, for numerical stability, the streamwise first derivative of pressure amplitude is neglected (note that the neglected first derivative is that of the slow-varying pressure amplitude, and not that of the overall pressure perturbation).[26]
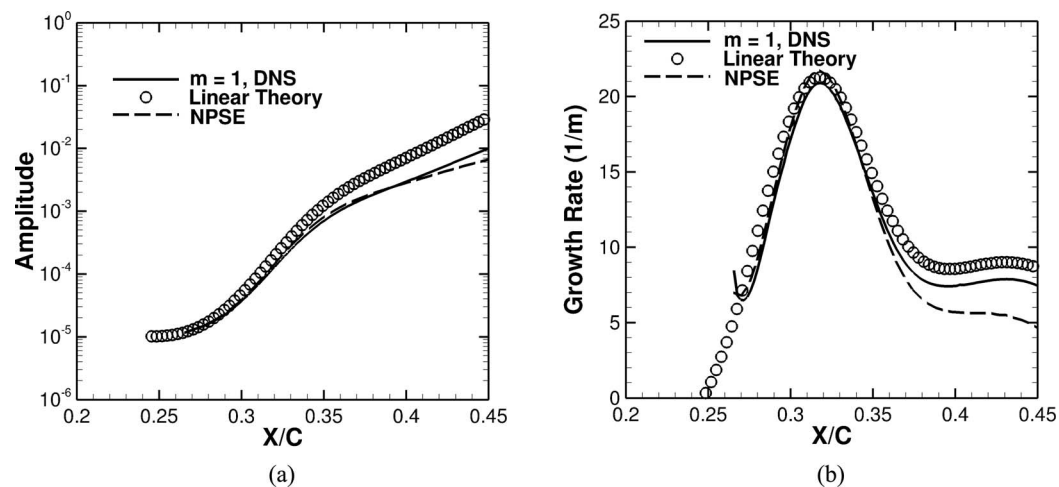

FIG. 10. Comparison of LSIT, NPSE, and DNS predictions for secondary wave evolution (primary wave: $\lambda_z = 8$ mm, $f = 1500$ Hz; secondary wave: $f = 13.5$ kHz, $A_{init} = 5 \times 10^{-7}$). (a) Fundamental amplitude of secondary wave. (b) Growth rate of secondary wave.

An equivalent but perhaps more revealing comparison between the LSIT, NPSE, and DNS predictions can be made by comparing the corresponding growth rates based on the peak chordwise velocity amplitude of the secondary instability mode (Figure 10(b)). In the main region of secondary mode amplification ($X/C < 0.37$), all three predictions are close to each other. To our knowledge, this result represents the first DNS based validation of secondary instability theory for traveling crossflow modes. The differences between the NPSE and DNS results within the above region are somewhat smaller than those relative to the LSIT predictions, except in the neighborhood of the peak growth rate location of the secondary mode. Therefore, the cause for the over-prediction of secondary instability growth by the LSIT method in this particular case may be related to the quasi-parallel assumption inherent to LSIT. However, this trend is certainly different from the analogous findings for the secondary instability of stationary crossflow modes.[16] Furthermore, the effects of a non-parallel basic state also tend to be destabilizing in the linear stability analysis of primary waves. Again, in this particular case, at least, an opposite trend appears to hold for the secondary instability evolution. Figure 10(b) also shows significant differences among the three different predictions for chordwise locations beyond the main region of secondary amplification ($X/C > 0.37$). The DNS prediction actually falls in between the LSIT and NPSE predictions.

3. Weakly nonlinear effects on secondary mode amplification

The growth and breakdown of secondary instability eventually lead to turbulence. In this process, as the amplitude of the secondary instability becomes progressively larger, its growth rate starts to deviate from that predicted by the linear theory due to the onset of nonlinear effects. Figure 11(a) shows the effect of initial secondary wave amplitude on the streamwise amplification of the fundamental secondary instability mode of Y/Z type and $f = 13\,500$ Hz corresponding to a finite amplitude primary crossflow disturbance with $\lambda_z = 8$ mm and $f = 1500$ Hz. The initial amplitude of the primary wave is fixed at 5×10^{-7} while the initial secondary wave amplitude is varied from 10^{-5} to 10^{-3}. In each case, the secondary wave amplitude is normalized by its initial value, so that the ordinate in Figure 11(a) corresponds to the growth factor relative to the inflow location. For the smallest secondary initial amplitude ($A_{init} = 10^{-5}$), the fundamental amplitude remains sufficiently small throughout the computational domain such that the instability growth may be considered to be linear. As the initial amplitude is increased, the amplitude growth eventually deviates from the linear theory. This occurs near $X/C \approx 0.44$ and 0.34 for $A_{init} = 10^{-4}$ and 10^{-3}, respectively; and in both cases, the fundamental mode amplitude is approximately 4% at the respective locations. The corresponding evolution of the mean wall shear in all three cases is shown in Figure 11(b). For larger
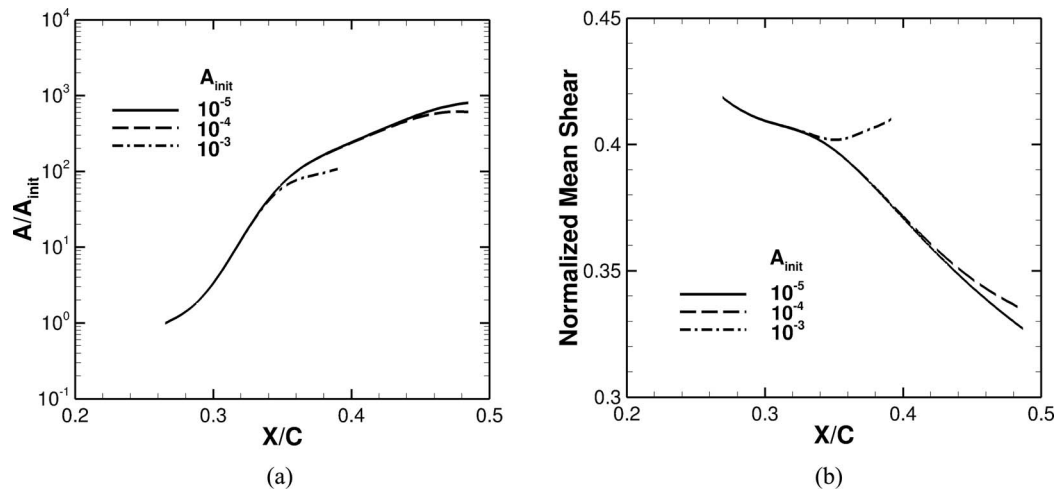

FIG. 11. Nonlinear evolution for selected initial amplitudes of the secondary wave. Secondary instability mode type: Y/Z; secondary instability frequency 13.5 kHz; primary wave spanwise wavelength: 8 mm; primary wave frequency: 1500 Hz; primary wave initial amplitude: 10^{-7}. (a) Amplitudes. (b) Mean wall shear.
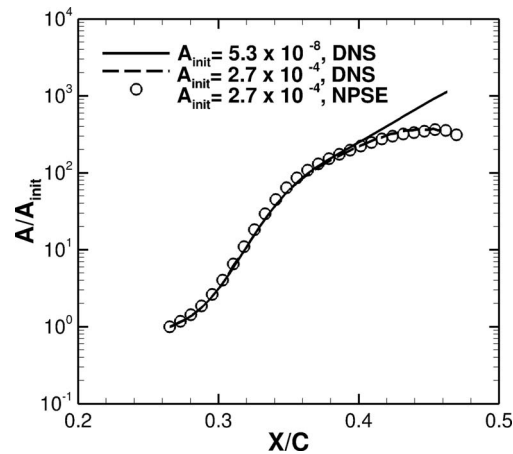
FIG. 12. Chordwise evolution of fundamental secondary mode for different initial amplitudes: Comparison between NPSE and DNS. Secondary instability mode type: Y/Z; secondary instability frequency 13.5 kHz; primary wave spanwise wavelength: 8 mm; primary wave frequency: 1500 Hz; primary wave initial amplitude: 10^{-7}.

initial amplitudes, the wall shear is higher. For largest initial amplitude, 10^{-3}, the wall shear begins a relatively rapid rise at $X/C = 0.36$, which may be indicative of the onset of transition.

The DNS result for secondary instability at larger initial amplitudes is next compared with the NPSE result along with the essentially linear DNS result of a much smaller initial amplitude. Figure 12 shows the amplitude curves for the fundamental frequency of the 13.5 kHz Y/Z mode. The amplitudes are normalized with their respective initial values so that all curves initially collapse onto each other. As amplitudes increase, the DNS curve with the larger initial amplitude starts to deviate from curve representing linear amplification due to nonlinear effects. The result of NPSE computation agrees well with the DNS result. The actual peak amplitude reached during the nonlinear evolution is approximately 10%, but no transition is observed before the end of the computational domain. However, the comparison confirms that NPSE should produce good results up to at least this amplitude, which should enable the NPSE method to be used with confidence in similar cases with much less demand on computational resources than DNS.

V. CONCLUDING REMARKS

This paper extends the previous studies of swept wing transition due to stationary crossflow instability by considering when traveling crossflow modes may dominate the transition process. When the initial amplitudes of the traveling crossflow vortices are comparable to those of the stationary modes for which the underlying boundary layer flow is modified strongly, the traveling crossflow vortices also support secondary instabilities in much the same way as the stationary crossflow modes. Computational results presented herein show that the traveling crossflow vortices saturate at much lower amplitudes than their stationary counterparts, approximately half the saturation amplitude for a stationary crossflow vortex with the same spanwise wavelength. However, despite of the lower amplitudes during the quasi-saturation stage, the growth of the secondary instabilities sustained by finite amplitude traveling crossflow vortices is at least as strong as the secondary modes of the stationary crossflow vortices.

The primary traveling crossflow vortex has a higher initial growth rate than the stationary mode, but saturates at significantly lower amplitudes. Additionally, the cross-plane velocity contours for the traveling mode case seem to lack the strong overturning structure of their stationary counterpart when viewed within an appropriately moving coordinate system. An interesting phenomenon is found in that the fundamental and mean flow correction modes appear to oscillate out of phase by approximately 90° to due the alternating stabilization and destabilization nonlinear interactions of the two modes.

Two dominant modes of secondary instability are found for the swept wing configuration investigated herein. The Y mode is dominant at large primary wave amplitudes, but its growth rates diminish faster than that of the Y/Z mode when the primary amplitude decreases. At smaller primary amplitudes of a $\lambda_z = 8$ mm traveling mode, the Y mode of secondary instability disappears all together, leaving a single, strongly amplifying Y/Z mode. The critical initial amplitudes enabling the 8 mm primary wave to sustain significant secondary amplification (i.e., secondary N-factors in excess of 4) have also been estimated for the swept wing configuration of interest. At lower initial amplitudes of the (primary) traveling crossflow modes, the dominant growth of secondary instability shifts to primary modes of larger spanwise wavelengths ($\lambda_z = 10$ mm and 12 mm, respectively). However, large N-factor values typical of those associated with the onset of transition in low disturbance environments are only achieved at far downstream locations. In that case, transition would appear more likely to occur as a result of stationary crossflow modes when the traveling crossflow mode amplitudes are at such low levels. Transition scenarios associated with the joint development of stationary and traveling crossflow modes will be investigated in future work.

Direct numerical simulations are carried out for a Y/Z-mode secondary instability of 13.5 kHz riding a 1500 Hz traveling crossflow vortex of 8 mm in spanwise wavelength. Comparisons with the predictions of both nonlinear parabolized stability equations and the linear secondary instability theory show that the linear secondary instability theory somewhat over predicts the growth of secondary instability in this particular case and the likely reason behind this discrepancy is the non-parallel effects associated with the underlying boundary layer flow.

ACKNOWLEDGMENTS

[1] D. I. A. Poll, "Transition in the infinite swept attachment line boundary layer," Aeronaut. Q. **30**, 607–629 (1979).

[2] M. R. Malik, F. Li, and C.-L. Chang, "Crossflow disturbances in three-dimensional boundary layers: nonlinear development, wave interaction and secondary instability," J. Fluid Mech. **268**, 1–36 (1994).

[3] M. R. Malik, F. Li, M. Choudhari, and C.-L. Chang, "Secondary instability of crossflow vortices and swept-wing boundary-layer transition," J. Fluid Mech. **399**, 85–115 (1999).

[4] M. Reibert, W. S. Saric, R. B. Carrillo, and K. L. Chapman, "Experiments in nonlinear saturation of stationary crossflow vortices in a swept-wing boundary layer," AIAA Paper No. 96-0184, 1996.

[5] M. Gaster, "A note on the relationship between temporarily increasing and spatially increasing disturbance in hydrodynamic instability," J. Fluid Mech. **14**, 222–224 (1962).

[6] W. Koch, F. P. Bertolotti, A. Stolte, and S. Hein, "Nonlinear equilibrium solutions in athree-dimensional boundary layer and their secondary stability," J. Fluid Mech. **406**, 131–174 (2000).

[7] M. Hogberg and D. Henningson, "Secondary instability of cross-flow vortices in Falkner–Skan–Cooke boundary layers," J. Fluid Mech. **368**, 339–357 (1998).

[8] G. Bonfigli and M. Kloker, "Secondary instability of crossflow vortices: validation of the stability theory by direct numerical simulation," J. Fluid Mech. **583**, 229–272 (2007).

[9] T. Friederich and M. Kloker, "Control of the secondary cross-flow Instability using localized suction," J. Fluid Mech. **706**, 470–495 (2012).

[10] Y. Kohama, W. S. Saric, and J. A. Hoos, "A high-frequency secondary instability of crossflow vortices that leads to transition," *Proceedings of the Royal Aeronautical Society Conference on Boundary Layer Transition and Control, London, UK* (Royal Aeronautical Society, 1991), pp. 4.1–4.13.

[11] S. Balachandar, C. L. Streett, and M. R. Malik, "Secondary instability in a rotating disk flow," J. Fluid Mech. **242**, 323–347 (1992).

[12] W. S. Saric, H. L. Reed, and E. B. White, "Stability and transition of three-dimensional boundary layers," Annu. Rev. Fluid Mech. **35**, 413–440 (2003).

[13] P. Wassermann and M. Kloker, "Mechanisms and passive control of crossflow-vortex-induced transition in a three-dimensional boundary layer," J. Fluid Mech. **456**, 49–84 (2002).

[14] H. Bippes, "Basic experiments on transition in three-dimensional boundary layers dominated by crossflow instability," Prog. Aerosp. Sci. **35**, 363–412 (1999).

[15] P. Wassermann and M. Kloker, "Transition mechanisms induced by traveling crossflow vortices in a three-dimensional boundary layer," J. Fluid Mech. **483**, 67–89 (2003).

[16] M. Choudhari, F. Li, L. Duan, M. H. Carpenter, C. L. Streett, and M. R. Malik, "Towards bridging the gap in hoslistic transtion prediction via numerical simulations," AIAA Paper 2013-2718, 2013.

[17] R. S. Down and E. B. White, "Free-stream turbulence and development of crossflow disturbances," J. Fluid Mech. **735**, 347–380 (2013).

[18] F. Li and M. Choudhari, "Spatially developing secondary instabilities and attachment line instability in supersonic boundary layers," AIAA Paper 2008-0590, 2008.

[19] F. Li and M. Choudhari, "Spatially developing secondary instabilities in compressible swept airfoil boundary layers," Theor. Comput. Fluid Dyn. **25**, 65–84 (2011).

[20] T. Herbert, "Secondary instability of boundary layers," Annu. Rev. Fluid Mech. **20**, 487–526 (1988).

[21] M. R. Malik, F. Li, and C.-L. Chang, "Nonlinear crossflow disturbances and secondary instability in three-dimensional boundary layers," *Proceedings of IUTAM Symposium* (Kluwer Acad. Publ., Manchester, UK, 1996), pp. 257–266.

[22] R. S. Lin and M. R. Malik, "On the stability of Attachment-line boundary layers. Part I. The incompressible swept Hiemenz flow," J. Fluid Mech. **311**, 239–255 (1996).

[23] M. Belisle, T. Neale, H. Reed, and W. Saric, "Design of a swept-wing laminar flow control floght experiment for transonic aircraft," AIAA Paper 2010-4381, 2010.

[24] Y.-S. Wie, "BLSTA – A boundary layer code for stability analysis," NASA CR 4481, 1992.

[25] W. S. Saric, "Flight experiments on swept-wing roughness receptivity: Phase 2. Feasibility of a laminar flow flight test," Phase 2, Year 1 Draft Report for AFOSR Grant No. FA955008-1-0475, June 2009.

[26] C.-L. Chang, "Langley stability and transition analysis code (LASTRAC) version 1.2 user manual," NASA/TM-2004-213233, June 2004.

[27] M. P. Martin, E. M. Taylor, M. Wu, and V. G. Weirs, "A bandwidth-optimized weno scheme for effective direct numerical simulations of compressible turbulence," J. Comput. Phys. **220**, 270–298 (2006).

[28] L. Duan, M. Choudhari, and F. Li, "Direct numerical simulation of crossflow-induced transition in a swept wing boundary layer," AIAA Paper 2013-2617, 2013.

[29] M. Choudhari, C.-L. Chang, C. L. Streett, and P. Balakumar, "Integrated transition prediction: A case study in supersonic laminar flow control," AIAA Paper 2003-0973, 2003.

[30] C.-L. Chang and M. M. Choudhari, "Boundary-layer receptivity and integrated transition prediction," AIAA Paper 2005-0526, 2005.

[31] F. Li, M. Choudhari, C.-L. Chang, C. L. Streett, and M. H. Carpenter, "Roughness based crossflow transition control: A computational assessment," AIAA Paper 2009-4105, 2009.

[32] F. Li, M. Choudhari, C.-L. Chang, C. L. Streett, and M. H. Carpenter, "Computational modeling of roughness-based laminar flow control on a subsonic swept wing," AIAA J. **49**(3), 520–529 (2011).

[33] M. R. Malik, W. Liao, F. Li, and M. Choudhari, "DRE-enhanced swept-wing natural laminar flow at high Reynolds numbers," AIAA Paper 2013-412, 2013.

[34] J. Gajjar, "On the nonlinear evolution of a stationary cross-flow vortex in a fully three-dimensional boundary layer flow," in *Proceedings of IUTAM Symposium on Nonlinear Instability and Transition in Three-Dimensional Boundary Layers, Manchester, UK*, edited by P. Duck and P. Hall (Kluwer, 1996), pp. 317–326.

[35] L. Jiang, M. Choudhari, C. Chang, and C. Liu, "Direct numerical simulations of crossflow disturbances in supersonic boundary layers," AIAA Paper 2004-589, 2004.

[36] M. Choudhari, "Roughness-induced generation of crossflow vortices in three-dimensional boundary layers," Theor. Comput. Fluid Dyn. **5**, 1–31 (1994).

[37] E. B. White and W. S. Saric, "Secondary instabilty of crossflow vortices," J. Fluid Mech. **525**, 275–308 (2005).